IEICE TRANSACTIONS

on Communications

VOL. E99-B NO. 6
JUNE 2016

The usage of this PDF file must comply with the IEICE Provisions on Copyright.
The author(s) can distribute this PDF file for research and educational (nonprofit) purposes only.
Distribution by anyone other than the author(s) is prohibited.

A PUBLICATION OF THE COMMUNICATIONS SOCIETY

The Institute of Electronics, Information and Communication Engineers
Kikai-Shinko-Kaikan Bldg., 5-8, Shibakoen 3chome, Minato-ku, TOKYO, 105-0011 JAPAN

PAPER Special Section on European ICT R&D Project Activities on Broadband Access Technologies in Conjunction with Main Topics of 2015 IEICE ICT Forum

Performance of All-Optical Amplify-and-Forward WDM/FSO Relaying Systems over Atmospheric Dispersive Turbulence Channels*

Phuc V. TRINH[†], ***Student Member***, **Ngoc T. DANG**[††], **Truong C. THANG**[†], ***Nonmembers***, ***and*** **Anh T. PHAM**[†a)], ***Member***

SUMMARY This paper newly proposes and theoretically analyzes the performance of multi-hop free-space optical (FSO) systems employing optical amplify-and-forward (OAF) relaying technique and wavelength division multiplexing (WDM). The proposed system can provide a low cost, low latency, high flexibility, and large bandwidth access network for multiple users in areas where installation of optical fiber is unfavorable. In WDM/FSO systems, WDM channels suffer from the interchannel crosstalk while FSO channels can be severely affected by the atmospheric turbulence. These impairments together with the accumulation of background and amplifying noises over multiple relays significantly degrade the overall system performance. To deal with this problem, the use of the M-ary pulse position modulation (M-PPM) together with the OAF relaying technique is advocated as a powerful remedy to mitigate the effects of atmospheric turbulence. For the performance analysis, we use a realistic model of Gaussian pulse propagation to investigate major atmospheric effects, including signal turbulence and pulse broadening. We qualitatively discuss the impact of various system parameters, including the required average transmitted powers per information bit corresponding to specific values of bit error rate (BER), transmission distance, number of relays, and turbulence strength. Our numerical results are also thoroughly validated by Monte-Carlo (M-C) simulations.

key words: *wavelength division multiplexing, free-space optics, optical amplify-and-forward, interchannel crosstalk, atmospheric turbulence, pulse broadening*

1. Introduction

Free-space optics (FSO) has recently received much attention in the first-mile access environment owing to a number of advantages over radio-frequency communications, including much higher bandwidth with license-free spectrum, better energy efficiency and possibly higher security. Compared to fiber optical communications, FSO also offers fiber-like data rate while being more flexible and cost-effective, as well as quicker and easier for deployment and re-deployment [1], [2]. Currently, wavelength division multiplexed (WDM) transmission, which allows to carry many separate and independent optical channels, can support Terabits per second capacities, and it can be easily integrated into FSO systems to considerably increase the bit rate [3]. This WDM/FSO combination is therefore a promising solution to meet the unprecedented growth in the global demand for broadband applications and services [4], [5]. In this paper, we propose a novel concept of all-optical access networks using multi-hop WDM/FSO to provide high-bandwidth connections for multiple users in an extended coverage. System performance is comprehensively analyzed taking into account crucial physical-layer impairments, including atmospheric attenuation, turbulence, interchannel crosstalk, and pulse broadening.

1.1 Related Studies and Motivations

Several WDM/FSO systems have been successfully demonstrated [3], [6]. WDM-Passive Optical Network (PON) using FSO in the distribution links to support multiple users at high bit rates is an appealing proposal [7]–[9]. In this hybrid WDM-PON/FSO network, the WDM channels suffer from interchannel crosstalk, while the FSO channels are affected by atmospherically induced scintillation, i.e., atmospheric turbulence. The combination of these two impairments results in turbulence-accentuated crosstalk effect, which severely degrades the overall system performance, particularly in the upstream transmission [8]. Practically, FSO could be an extension of optical fiber since both links share the identical transmission wavelengths and system components. Especially, using a pair of FSO terminals (FSOT), which can be transparently connected to single-mode fiber lines, FSO systems can be fully compatible with optical fiber networks [10].

FSO nevertheless is confined to short-haul applications since its reliability is degraded due to the distance-dependent atmospheric turbulence-induced fading and loss [11]. To extend the coverage of FSO systems, relaying FSO has been considered as a suitable solution [12]–[18]. Many previous studies mainly focused on electrical relaying, where all signal processes are implemented in the electrical domain [12]–[14]. This technique is daunting from an implementation perspective for Gigabit per second (Gbps)-rate FSO links since it requires complex optoelectronics and decoding/encoding hardware. Therefore, the all-optical relaying technique, i.e., optical amplify-and-forward (OAF), where the signal processing is only performed in the optical

Manuscript received August 27, 2015.
Manuscript revised January 28, 2016.

[†]The authors are with the Computer Communications Lab., University of Aizu, Aizuwakamatsu-shi, 965-8580 Japan.
[††]The author is with the Department of Optical Communications, Posts and Telecommunications Institute of Technology, Hanoi, 100000 Vietnam.

*The paper was presented in part at IEEE/IET CSNDSP'14.

a) E-mail: pham@u-aizu.ac.jp

DOI: 10.1587/transcom.2015EUP0004

Copyright © 2016 The Institute of Electronics, Information and Communication Engineers

domain so that the full bandwidth of an optical signal can be used, has been recently studied [15]–[18]. It is generally deduced from these studies that OAF relaying is faster and simpler to implement and achieves a better performance than electrical relaying unless the number of relays is large, in which case the accumulation of background and amplified spontaneous emission (ASE) noises impose a negative impact on the system performance.

On the other hand, the signal dispersion (pulse broadening) is another important factor in FSO system performance. In recent studies, the Gaussian pulse propagation model was employed so that both atmospheric turbulence and pulse broadening could be investigated in the performance of FSO systems [19], [20]. However, the pulse broadening issue has not been clarified in WDM/FSO systems.

1.2 Main Contributions

The main contributions in this paper can be summarized as follows.

First, we propose a novel concept of all-optical access networks using multi-hop WDM/FSO to provide high-bandwidth connections for multiple users. This proposition takes advantage of both the all-optical relaying technique and the WDM transmission, hence resulting in a low cost, reliable, flexible, and high-speed access network. This proposed network can be compatibly combined with the pre-deployed fiber network to further increase the network coverage. Therefore, it could be a realistic solution for the first-mile 'bottleneck' problem, especially when fiber installation is not favorable.

Secondly, we employ the M-ary pulse position modulation (M-PPM) combined with the OAF relaying technique to combat against the turbulence-accentuated inter-channel crosstalk effect, which is the main impairment in WDM/FSO systems. In previous studies, M-PPM has been employed as an energy-efficient transmission method [21]–[23]. Additionally, the use of PPM also avoids adaptive threshold adjustments required in on-off keying (OOK) [24].

Thirdly, for performance analysis, we take into account effects of all noises and atmospheric impairments, including turbulence and pulse broadening. The atmospheric turbulence is modeled by a Gamma-Gamma channel, which is suitable for a wide range of turbulence conditions [25], while the pulse broadening is characterized by the Gaussian pulse propagation model. Our numerical results, which are validated by Monte-Carlo (M-C) simulations, show that the proposed WDM/FSO system using PPM combined with OAF relaying technique is a feasible solution for optical access networks.

2. Proposed System Descriptions

2.1 Network Model

Figure 1(a) shows the model of a typical PON using optical fiber links, which consists of optical network units (ONUs),

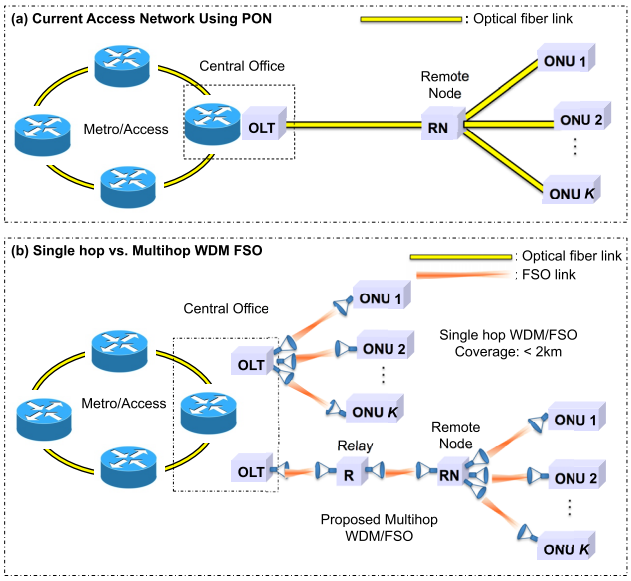

Fig. 1 (a) PON optical fiber access network; (b) Proposed all-optical multi-hop WDM/FSO access network.

a passive splitter at the remote node (RN), and an optical line terminal (OLT). Typically, PON can reach the distance of up to 20 km, and it is capable of delivering upstream to 1.2 Gbps and 2.4 Gbps downstream to the port with current standards [26]. As the next step in fiber access evolution, the ITU-T is defining the second next generation PON (NG-PON2), which is primarily based on time and wavelength division multiplexing (TWDM) since it is most compatible with the high volume residential application. The NG-PON2 could offer 40 Gbps aggregate downstream capacity and 10 Gbps upstream [27]. Nevertheless, it is not always economical or possible to have optical fiber installation due to the high cost, especially in vast, low-density remote areas, difficult terrains, the limitation of running additional cables (such as city centers, historical areas), or the need of temporary connection only. A solution for these issues is to use FSO instead of the optical fiber [8], [9]. As shown in the upper part of Fig. 1(b), FSO is combined with WDM/PON to form a hybrid optical access network with lower cost and higher flexibility. The coverage of single-hop FSO links in the distribution network is however limited (to about 2 kilometers) due to the negative impacts of atmospheric and weather conditions [8].

To address above-mentioned issues, we propose a cost-effective, flexible, and reliable network model using multi-hop WDM/FSO, as shown in the lower part of Fig. 1(b). For the extended distance from the OLT to the RN, multi-hop WDM/FSO relaying with erbium-doped fiber amplifiers (EDFAs) is employed. In this WDM/FSO network, FSO links can be configured in different topologies, such as point-to-point, point-to-multipoint, ring, or mesh connections. The cost of deploying WDM/FSO network can be significantly lower than that of conventional PONs because no fibers are required between the OLT and service areas, lead-

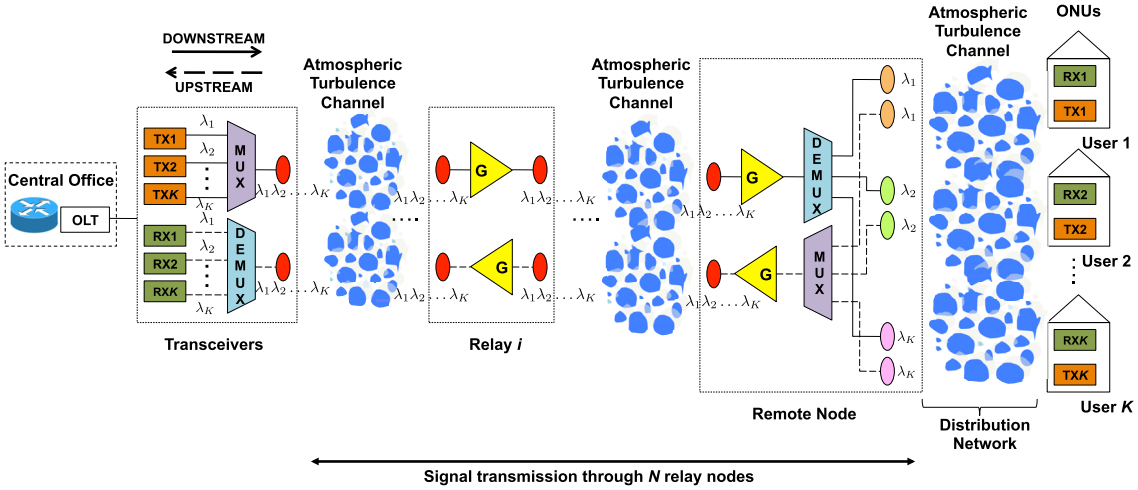

Fig. 2 Multi-hop OAF relaying WDM/FSO systems for optical access networks.

ing to a substantial reduction of fiber installation and maintenance expenses. Besides, the WDM/FSO systems can be fully compatible with the terrestrial fiber communication in metro networks, which provide not only the multi-gigabit link capacity but also the link stability and reliability [10]. Moreover, based on full-optical FSO systems, advanced Radio over FSO (RoFSO) systems have also been developed with the capability of transferring multiple wireless signals using WDM/FSO channels [28]. Above-mentioned advantages make our proposed multi-hop WDM/FSO system become a promising solution for all-optical access networks.

2.2 System Model

For performance analysis purpose, we use a model of multi-hop OAF relaying WDM/FSO access network shown in Fig. 2. For both downstream and upstream directions, the OLT communicates with ONUs through N intermediate relays (R_i, $i = 1, 2, \ldots, N$), including the RN. The total transmission distance is $L = \sum_{i=1}^{N+1} d_i$, where d_i is the transmission distance from the $(i-1)$-th node to the i-th node (with node 0 is the OLT and node $N+1$ is the ONU).

In the downstream transmission, signals from K transmitters, each with an unique wavelength $(\lambda_1, \lambda_2, \cdots, \lambda_K)$ are combined by a WDM mux and then transmitted via multi-hop FSO channels to the RN. The optical wavelengths are chosen in the C band (i.e., around 1550 nm) with channel spacing of 100 GHz, since 1550 nm light suffers from less atmospheric attenuation and it is suitable for EDFA technology and high quality transceivers [29]. At each relay node, an optical amplifier (EDFA) is used to directly amplify the optical signals. A single EDFA can simultaneously amplify many data channels at different wavelengths within the gain region. However, the advantage of an optical amplifier comes at the cost of introducing ASE noise, which somewhat offsets the performance gain. After that, at the RN, WDM demux separates the multiplexed optical signals into constituent wavelengths. Due to the defectiveness of the demux and transmitting lenses at the RN, the end-user may receive the optical signal of undesired wavelengths, i.e., interferers. This phenomenon is also known as interchannel crosstalk, which was previously studied in [29], [30]. There also exists several losses of mux/demux, which comprise the signal mux, demux losses (denoted as L_{mx}, L_{dx}, respectively), and $L_{dx,XT}$, which indicates the crosstalk level from the interferer at the demux. Finally, in the distribution network, signals with constituent wavelengths are delivered to the corresponding end-users (ONUs) in a point-to-point scheme. At each receiver, PIN photodiode is used to convert the electrical field into the photocurrent.

In the upstream direction, interchannel crosstalk arises due to the imperfection of the demux at the OLT when separating different wavelengths to corresponding receivers. However, the interchannel crosstalk effect in this situation becomes more severe, since the atmospheric turbulence in the distribution network results in a fluctuating crosstalk effect. It is also called as the turbulence-accentuated interchannel crosstalk, which arises when the signal and crosstalk paths are independently turbulent, i.e., physically totally distinct, as in the case of the upstream. The effect of turbulence-accentuated interchannel crosstalk in WDM-PON integrated with FSO networks was investigated in [8]. It is also worthy to note that there may exist intrachannel crosstalk in the upstream transmission if a portion of the transmitted power falls in the field of view of an unexpected receiving lens due to the beam spreading effect. Nevertheless, intrachannel crosstalk can be neglected, since we can generally arrange the position of ONUs to avoid the near identical transmission paths.

For each wavelength, M-ary PPM scheme is employed. At the transmitter, input data is first modulated at a PPM modulator, where each block of b bits is mapped to one of M possible symbols $(s_0, s_1, ..., s_M)$, where $M = 2^b$. The symbol interval, T_w, is divided into M time-disjoint time slots and an electrical pulse is sent in one of these M time slots while remaining $(M-1)$ time slots are empty. This pulse is then converted into an optical pulse with constant power of $P_{t,sig}$ by a laser diode. Denoting R_b as the bit rate of the system,

the symbol interval has a duration given by $T_w = \frac{b}{R_b} = \frac{\log_2 M}{R_b}$, and time slots have the duration of $T_s = \frac{T_w}{M}$.

At the input of each relay, optical signals include not only data signal but also background noise and interferer signal with the average powers of P_b and $P_{t,int}$, respectively. Here, the case of a single interferer is assumed. These signals are amplified by an EDFA with the fixed gain G, which is set to keep the average relay output power constant at $P_{t,sig}$ [15], [16]. The signals are then transmitted to the next relay together with ASE noise, which can be described by additive zero-mean white Gaussian model with the optical power given by $P_A = h_P f\,(G-1)\,n_{sp}B_0$, where h_P is the Planck's constant, f is the frequency, n_{sp} is the amplifier spontaneous emission parameter, and B_0 is the optical bandwidth [31]. Over multiple relays, background and ASE noises are amplified and accumulated.

At the destination, the received signal, including the background noise at the receiver, is converted into the photocurrent by a PIN photodetector. Next, integrated photocurrents over M time slots are compared at the PPM demodulator to find the position of the slot with the highest current, which determines the transmitted symbol. Finally, detected symbol is converted to the binary data by a symbol-to-bit converter.

3. FSO Dispersive Turbulence Channel Model

This section presents the mathematical model of FSO channel with h_i, $(i = 1, 2, \cdots, N+1)$, which is the channel state modeling the random attenuation of the propagation channel between the $(i-1)$-th node and the i-th node. In the proposed system, each hop is assumed to be equidistant (i.e., $d_1 = \cdots = d_i = \cdots = d_{N+1} = \frac{L}{N+1}$), and the channel state between every pair of relays is considered to be independent and identically distributed. In our model, h_i arises due to two factors: channel loss (h_i^l) including the geometric spreading of the optical beam, atmospheric attenuation, and pulse broadening; and atmospheric turbulence (h_i^a). The channel coefficient hence can be described as $h_i = h_i^l h_i^a$.

3.1 Atmospheric Dispersive Model

To evaluate time-domain spreading of a pulse wave propagating through atmospheric turbulence, we assume that the transmitted waveform in each PPM time slot is a Gaussian pulse. The amplitude of the Gaussian pulse is described by

$$U_t(t) = \sqrt{P_0}\exp\left(-\frac{t^2}{T_0^2}\right), \tag{1}$$

where P_0 and T_0 are the average power and the half-width (at the $1/e$ point) of the input pulse, respectively [32]. The relation between the average power of Gaussian pulse (P_0) and the average power per time slot ($P_{t,sig}$) is given by

$$P_0 = \frac{\sqrt{2}T_s}{\sqrt{\pi}T_0}P_{t,sig}, \tag{2}$$

where T_s is the duration of the time slot [19].

Over a transmission distance d_i, the received optical signal is attenuated by the propagation loss including the geometrical spreading of the optical beam and atmospheric attenuation. It is easy to obtain the value of loss due to geometric spreading as a function of the area of the receiver aperture A and the angle of divergence θ. On the other hand, the atmospheric attenuation can be described by the exponential Beer-Lambert's law. As a result, the total of atmospheric attenuation and geometric spreading can be formulated as

$$a_{att} = \frac{A}{\pi\left(\frac{\theta}{2}d_i\right)^2}\exp(-a_l d_i), \tag{3}$$

where $A = \pi(a)^2$ with a is the radius of the receiver aperture, and a_l is the atmospheric attenuation coefficient. In addition, the optical pulse obtained at the receiver is broadened due to the atmospheric turbulence, and its average power is reduced. Therefore, the received signal at the distance of d_i meters from the transmitter, taking into consideration the effects of geometrical spreading of the optical beam, atmospheric attenuation, and pulse broadening, can be mathematically expressed as [19]

$$U_r(t) = \sqrt{P_0 a_{att}}\frac{T_0}{\sqrt{T_0^2+8\delta}}\exp\left(-\frac{t^2}{T_0^2+8\delta}\right). \tag{4}$$

The parameter δ, which governs the scale of pulse broadening and average power reduction, is given by $\delta = \frac{0.3908C_n^2 d_i L_0^{5/3}}{c^2}$, where C_n^2 stands for the altitude-dependent index of the refractive structure parameter, and L_0 is the outer scale of turbulence, and c is the light velocity [32].

As pulse is spread out of the time slot owing to pulse broadening, the average power per PPM time slot at the receiver (P_r) is reduced compared to $P_{t,sig}$. Therefore, the power loss coefficient caused by atmospheric attenuation and pulse broadening can be determined by

$$h_i^l = \frac{P_r}{P_{t,sig}} = \frac{1}{P_{t,sig}T_s}\int_{-T_s/2}^{T_s/2}|U_r(t)|^2\,dt. \tag{5}$$

3.2 Atmospheric Turbulence Model

An optical wave propagating through the atmosphere will experience irradiance (i.e., intensity) fluctuations, or scintillation. Scintillation is caused by the inhomogeneities in the temperature and pressure of the atmosphere leading to refractive index variations (i.e., atmospheric turbulence). To characterize the whole range of atmospheric turbulence effects (i.e., weak, moderate, and strong), Gamma-Gamma (G-G) distribution has been found to be a suitable choice since it is able to model both small-scale and large-scale fluctuations [25]. The G-G probability density function (pdf) of $h_i^a > 0$ is given as

$$f_{h_i^a}(h_i^a) = \frac{2\,(\alpha\beta)^{(\alpha+\beta)/2}}{\Gamma(\alpha)\,\Gamma(\beta)}(h_i^a)^{\frac{\alpha+\beta}{2}-1} \times K_{\alpha-\beta}\left(2\sqrt{\alpha\beta h_i^a}\right), \tag{6}$$

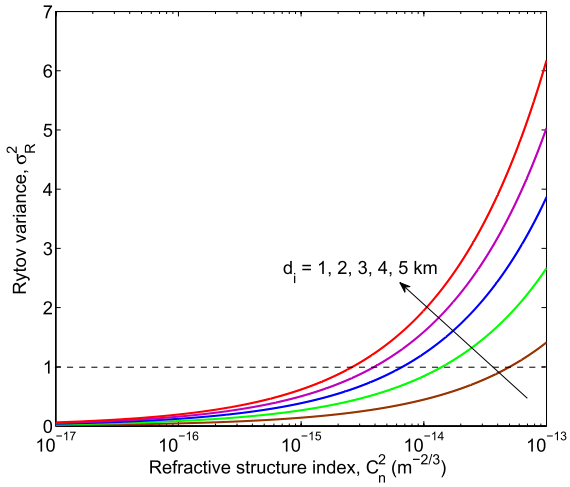

Fig. 3 Rytov variance versus the refractive structure index for different transmission distances.

where $\Gamma(\cdot)$ denotes Gamma function defined as $\Gamma(w) \triangleq \int_0^\infty t^{w-1}e^{(-t)}dt$, $K_{\alpha-\beta}(\cdot)$ is the modified Bessel function of the second kind of order $(\alpha-\beta)$, $\alpha > 0$ and $\beta > 0$ are the effective numbers of small-scale and large-scale eddies of scattering environment, respectively. Assuming a plane wave propagation of the optical beam, α and β are given as

$$\alpha \cong \left[\exp\left(\frac{0.49\sigma_R^2}{(1+1.11\sigma_R^{12/5})^{7/6}}\right)-1\right]^{-1}, \tag{7}$$

$$\beta \cong \left[\exp\left(\frac{0.51\sigma_R^2}{(1+0.69\sigma_R^{12/5})^{5/6}}\right)-1\right]^{-1}, \tag{8}$$

where σ_R^2 is the Rytov variance which is defined as

$$\sigma_R^2 \triangleq 1.23\left(\frac{2\pi}{\lambda}\right)^{7/6} C_n^2 d_i^{11/6}, \tag{9}$$

with λ is the optical wavelength [25]. In general, C_n^2 varies from 10^{-13} $m^{-2/3}$ to 10^{-17} $m^{-2/3}$ [33], and a table reporting C_n^2 for different weather conditions can be found in [34]. Illustratively, Fig. 3 shows the Rytov variance σ_R^2 versus C_n^2 for different transmission distances. Typically, weak, moderate, and strong turbulence conditions respectively correspond to $\sigma_R^2 < 1$, $\sigma_R^2 \approx 1$, and $\sigma_R^2 > 1$. The saturation regime is defined by $\sigma_R^2 \to \infty$ [35].

4. Bit-Error Rate Analysis

Once the PPM symbol is detected, it is mapped to a string of $\log_2(M)$ bits via the inverse of the encoding mapping. There are $M/2$ symbol errors that will produce an error in a given bit in the string, and there are $(M-1)$ unique symbol errors. Thus, assuming all symbol errors are equally likely, and denoting P_e as the symbol error probability (SEP), the bit error rate (BER) of the system then can be derived as

$$\text{BER} = \frac{M}{2(M-1)}P_e. \tag{10}$$

We assume that the transmitted data is large enough that the probabilities of sending any symbols are the same. At the receiver, the photocurrent I_u corresponds to the u-th slot ($0 \le u \le M-1$) of the received symbol. Without the loss of generality, we assume that symbol s_0 is transmitted, i.e., I_0 is the signal current corresponding to the signal slot (slot 0).

In the downstream direction, the signal and interferer can be assumed to experience the same atmospheric turbulence as the crosstalk arises before the distribution link (i.e., $(N+1)$-th hop). The downstream interchannel crosstalk is not turbulence-accentuated since it traverses the same atmospheric path as the signal (neglecting slight wavelength difference impact on σ_R^2). Hence, the G-G pdfs for both signal and interferer can be considered to be the same. Applying the union bound, the SEP for the downstream transmission can be expressed as

$$\begin{aligned} P_e &\le 1 - \Pr\{I_0 > I_u | u \in \{1,...,M-1\}, s = s_0\} \\ &\le (M-1)\Pr\{I_0 \le I_u | u \in \{1,...,M-1\}, s = s_0\} \\ &\le \frac{M-1}{2}\int_0^\infty dh_1^a \cdots \int_0^\infty dh_i^a \cdots \int_0^\infty dh_{N+1}^a \\ &\quad f_{h_1^a}\left(h_1^a\right)\cdots f_{h_i^a}(h_i^a)\cdots f_{h_{N+1}^a}\left(h_{N+1}^a\right)\text{erfc}\left(\sqrt{\frac{\text{SNR}}{2}}\right). \end{aligned} \tag{11}$$

In the upstream direction, the signal and interferer first travel over physically distinct paths in the $(N+1)$-th hop (from ONUs to the RN). Therefore, their G-G distributions can be assumed to be independent. In our analysis, the channel states of the $(N+1)$-th hop for signal and interferer are denoted as $h_{N+1,sig} = h_{N+1,sig}^l h_{N+1,sig}^a$ and $h_{N+1,int} = h_{N+1,int}^l h_{N+1,int}^a$, respectively. Similarly, the upper bound of the SEP for the upstream transmission can be expressed as

$$\begin{aligned} P_e \le{}& \frac{M-1}{2}\int_0^\infty dh_1^a \cdots \int_0^\infty dh_i^a \cdots \int_0^\infty dh_{N+1}^a \int_0^\infty dh_{N+1,int}^a \\ & f_{h_1^a}\left(h_1^a\right)\cdots f_{h_i^a}(h_i^a)\cdots f_{h_{N+1,sig}^a}\left(h_{N+1,sig}^a\right) \\ & \times f_{h_{N+1,int}^a}\left(h_{N+1,int}^a\right)\text{erfc}\left(\sqrt{\frac{\text{SNR}}{2}}\right). \end{aligned} \tag{12}$$

In (11) and (12), $\Pr\{\cdot\}$ denotes the probability of the given event, s represents the transmitted symbol and $\text{erfc}(z) \triangleq \frac{2}{\sqrt{\pi}}\int_z^\infty e^{-t^2}dt$ is the complementary error function. Following (6), $f_{h_i^a}\left(h_i^a\right)$ is the G-G pdf of h_i^a of the i-th hop for the signal ($i = 1, 2, \cdots, N+1$), and $f_{h_{N+1,int}^a}\left(h_{N+1,int}^a\right)$ is the G-G pdf of $h_{N+1,int}^a$ of the $(N+1)$-th hop for the interferer. SNR is the electrical signal to noise ratio in case of PPM signaling, which is defined as

$$\text{SNR} = \frac{(\mu_0 - \mu_u)^2}{\sigma_0^2 + \sigma_u^2}. \tag{13}$$

In (13), σ_0^2 and σ_u^2 are receiver noise variances of signal currents in 0 and u slots, which can be expressed as

$$\begin{bmatrix}\sigma_0^2\\ \sigma_u^2\end{bmatrix}=\begin{bmatrix}\sigma_{sig}^2+\sigma_{int}^2+\sigma_{b,r}^2+\sigma_{ASE,r}^2+\sigma_{b,d}^2+\sigma_{ASE,d}^2+\sigma_T^2\\ \sigma_{int}^2+\sigma_{b,r}^2+\sigma_{ASE,r}^2+\sigma_{b,d}^2+\sigma_{ASE,d}^2+\sigma_T^2\end{bmatrix}, \tag{14}$$

where σ_{sig}^2, σ_{int}^2, $\sigma_{b,r}^2$, $\sigma_{ASE,r}^2$, $\sigma_{b,d}^2$, $\sigma_{ASE,d}^2$, and σ_T^2 are variances of signal shot noise, interferer shot noise, accumulated amplified background noise over multiple relays, accumulated amplified ASE noise over multiple relays, background noise at the destination, ASE noise resulted from the amplifier at the RN received at the destination, and receiver thermal noise, respectively. $\mu_0 = I_{sig} + I_{int}$ and $\mu_u = I_{int}$ are respectively the mean values of signal currents in 0 and u slots, in which I_{sig} and I_{int} are the signal and interferer currents.

Since the atmospheric turbulence in the $(N+1)$-th hop is treated similarly in the downstream direction and independently in the upstream direction for the signal and interferer, the calculation of signal and interferer currents as well as receiver noise variances is derived differently.

4.1 Downstream Analysis

For the downstream transmission, I_{sig} and I_{int} can be expressed as

$$\begin{bmatrix}I_{sig}\\ I_{int}\end{bmatrix}=\begin{bmatrix}\Re P_{t,sig}\left(\prod_{i=1}^{N} G_i h_i^l h_i^a\right) h_{N+1}^l h_{N+1}^a L_{mx} L_{dx}\\ \Re P_{t,int}\left(\prod_{i=1}^{N} G_i h_i^l h_i^a\right) h_{N+1}^l h_{N+1}^a L_{mx} L_{dx} L_{dx,XT}\end{bmatrix}, \tag{15}$$

where $\Re$ is the responsivity of the PIN photodiode, G_i is the optical amplifier fixed-gain at the i-th relay (assuming that $G_1 = \cdots = G_i = \cdots = G_N$). In (14), the variances of receiver noises can be expressed as

$$\sigma_{sig}^2 = 2q\Re P_{t,sig}\left(\prod_{i=1}^{N} G_i h_i^l h_i^a\right) h_{N+1}^l h_{N+1}^a L_{mx} L_{dx} B_e, \tag{16}$$

$$\sigma_{int}^2 = 2q\Re P_{t,int}\left(\prod_{i=1}^{N} G_i h_i^l h_i^a\right) h_{N+1}^l h_{N+1}^a L_{mx} L_{dx} L_{dx,XT} B_e, \tag{17}$$

$$\sigma_{b,r}^2 = 2q\Re P_b\left(\sum_{i=1}^{N}\prod_{k=i}^{N} G_k h_{k+1}^l h_{k+1}^a\right) L_{dx} B_e, \tag{18}$$

$$\sigma_{ASE,r}^2 = 2q\Re\left(\sum_{i=1}^{N-1}\prod_{k=i+1}^{N} G_k h_k^l h_k^a h_{N+1}^l h_{N+1}^a P_A^i\right) L_{dx} B_e, \tag{19}$$

$$\sigma_{ASE,d}^2 = 2q\Re P_A^{N+1} h_{N+1}^l h_{N+1}^a L_{dx} B_e, \tag{20}$$

$$\sigma_{b,d}^2 = 2q\Re P_b B_e, \tag{21}$$

$$\sigma_T^2 = \frac{4k_B T}{R_L} B_e, \tag{22}$$

where q is the electron charge; k_B is the Boltzmann's constant; T is the absolute temperature; R_L is the load resistance; B_e is the effective noise bandwidth defined as $B_e = \frac{1}{T_s} = \frac{MR_b}{\log_2(M)}$; P_A^i is the average power of ASE noise at the i-th relay, assuming that $P_A^1 = \cdots = P_A^i = \cdots = P_A^N$.

4.2 Upstream Analysis

By substituting $h_{N+1,sig}^l h_{N+1,sig}^a$ and $h_{N+1,int}^l h_{N+1,int}^a$ for $h_{N+1}^l h_{N+1}^a$ from (15) to (17), we respectively obtain I_{sig}, I_{int}, and σ_{sig}^2, σ_{int}^2 for the upstream transmission. To obtain $\sigma_{ASE,d}^2$, $h_{N+1}^l h_{N+1}^a$ in (20) is replaced by $h_1 = h_1^l h_1^a$ because this ASE noise experiences turbulence from the first hop when considering the direction from ONUs to the OLT. For $\sigma_{b,r}^2$, $\sigma_{ASE,r}^2$, $\sigma_{b,d}^2$, and σ_T^2, the calculation is the same as in (18), (19), (21), and (22), respectively.

5. Numerical Results

In this section, we numerically investigate the BER of the proposed system under the assumption of a single interferer for both downstream and upstream transmissions. The derivation of closed-form expression for BER is relatively complex when all noises (including signal dependent ones) and interference are considered. In some special cases, when noise is assumed as signal independent Gaussian, the closed-form expression for BER can be derived [12], [13]. In this study, we base on exact-form upper bound expressions shown in (11) and (12) to investigate the BER for both cases of the upstream and the downstream. M-C simulations are also performed to validate the tight upper bound analysis.

It is noted that, for a fair comparison, the performance of the proposed system is examined under a constraint on the average power per information bit; that means, the average transmitted power of the PPM symbol, $P_{t,sig}$ can be given by $P_{t,sig} = (M \log_2 M) P_s$ with P_s is the average transmitted power per information bit. The required P_s here is considered for achieving the BER of 10^{-6} so that the operational performance (when BER = 10^{-9}) can be achieved when forward error correction (FEC) is applied. For the downstream transmission, the signal and interferer are assumed to have the same launch average power ($P_{t,sig} = P_{t,int}$) and distance to RN. On the contrary, in the upstream transmission, we also assume $P_{t,sig} = P_{t,int}$ but the distances to RN from the signal and interferer are separately examined. The system parameters and constants used in the analysis are shown in Table 1.

5.1 Downstream Transmission

First, Fig. 4(a) and Fig. 4(b) show BER versus P_s for the downstream transmission in cases of OOK and 4-PPM with different numbers of relays N within a fixed distance of 4 km. It is confirmed that the system performance could be significantly improved by increasing N. In Fig. 4(a) for systems using OOK, when N increases from 1 to 2 relays, 2 to 3 relays, and 3 to 4 relays, the performance improvements are 7 dB, 4 dB, and 2.5 dB, respectively. The decrease of the performance improvements is due to the accumulation of

Table 1 System parameters and constants.

Name	Symbol	Value
Boltzmann's constant	k_B	1.38×10^{-23} W/K/Hz
Planck's constant	h_P	6.626×10^{-34}
Electron charge	q	1.6×10^{-19} C
Optical bandwidth	B_0	125 GHz
Load resistor	R_L	50 Ω
Receiver temperature	T	300 K
PD responsivity	$\Re$	1 A/W
ASE parameter	n_{sp}	5
Attenuation coefficient	a_l	0.1 dB/km
Receiver radius	a	10 cm
Divergence angle	θ	1 mrad
Background power	P_b	−40 dBm
Wavelength	λ	1550 nm
Mux loss	L_{mx}	−3.5 dB
Demux loss	L_{dx}	−3.5 dB

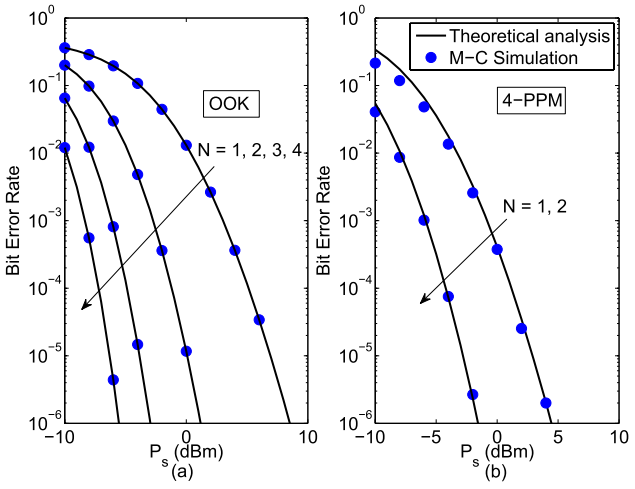

Fig. 4 Downstream transmission: BER versus the average transmitted power per information bit P_s, with 4-PPM, $R_b = 1$ Gbps, $L_{dx,XT} = -30$ dB, $L = 4$ km, and $C_n^2 = 5 \times 10^{-15}$ for different numbers of relays N in systems using OOK (a) and 4-PPM (b).

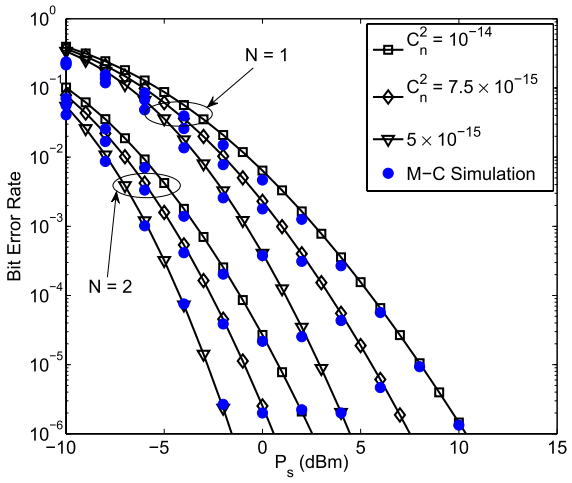

Fig. 5 Downstream transmission: BER versus the average transmitted power per information bit P_s, with 4-PPM, $R_b = 1$ Gbps, $L_{dx,XT} = -30$ dB, and $L = 4$ km, for different turbulence strengths C_n^2.

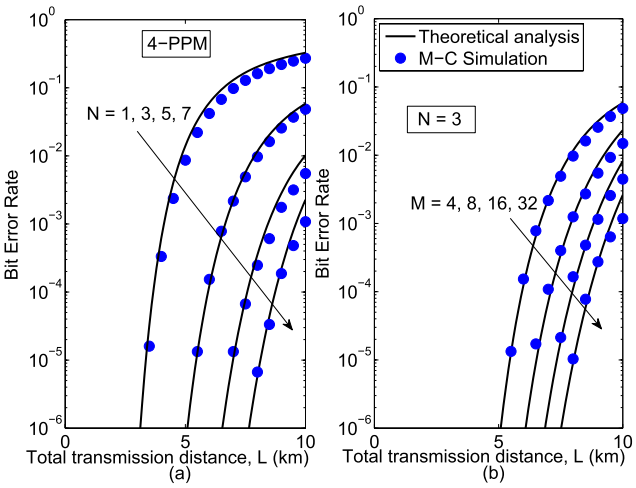

Fig. 6 Downstream transmission: BER versus the transmission distance L, $P_s = 0$ dBm, $R_b = 1$ Gbps, $L_{dx,XT} = -30$ dB, and $C_n^2 = 5 \times 10^{-15}$ for different numbers of relays (a) and orders of PPM modulation (b).

amplified background and ASE noises over multiple relays. On the other hand, in Fig. 4(b) for systems using 4-PPM, it is observed that PPM-based systems outperform OOK-based ones. Compared to OOK-based systems with the cases of $N = 1$ and $N = 2$, PPM-based systems attain the performance improvements of 4 dB and 3 dB, respectively. Therefore, PPM combined with OAF relaying is a good solution to improve the system performance, avoiding the adaptive threshold required in optimum-performing OOK-modulated FSO systems.

Next, Fig. 5 illustrates BER of the proposed system using 4-PPM versus P_s for the downstream transmission with various turbulence strengths. Within the total distance of 4 km, the BER performance is constantly deteriorated when the turbulence becomes stronger (i.e., higher C_n^2). With only one relay, the required P_s to attain BER of 10^{-6} are 10.5 dBm, 7.5 dBm, and 4.5 dBm corresponding to C_n^2 of 10^{-14}, 7.5×10^{-15}, and 5×10^{-15}. With two relays, the BER performance is significantly improved. More specifically, compared to the case when $N = 1$, the performance improvements when $N = 2$ are 8 dB, 7 dB, and 6 dB for C_n^2 of 10^{-14}, 7.5×10^{-15}, and 5×10^{-15}, respectively.

In Fig. 6, we investigate BER versus the total transmission distance for different numbers of relays (Fig. 6(a)) and orders of PPM scheme (Fig. 6(b)). In Fig. 6(a), the total transmission distance L could be further increased by increasing N. For instance, using 4-PPM, the maximum distances (calculated at BER = 10^{-6}) achieved with $N = 1$, $N = 3$, $N = 5$, and $N = 7$ are 3 km, 5 km, 6.5 km, and 7.6 km, respectively. It is also noticed that the distance improvements decrease with the increase of N due to background and ASE noises accumulation, for example, the distance improvements are 2 km, 1.5 km, and 1.1 km, when N is increased from 1 to 3, 3 to 5, and 5 to 7, respectively. However, it is not always economically or technically feasible to deploy additional relays. Therefore, another choice to improve the transmission distance is to increase the mod-

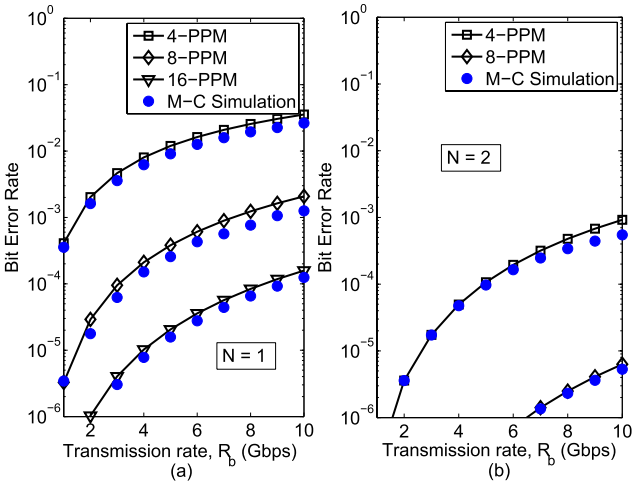

Fig. 7 Downstream transmission: BER versus the transmission rate R_b, $P_s = 0\,\text{dBm}$, $L_{dx,XT} = -30\,\text{dB}$, and $C_n^2 = 5 \times 10^{-15}$, and $L = 4\,\text{km}$ for different orders of PPM modulation with $N = 1$ (a) and $N = 2$ (b).

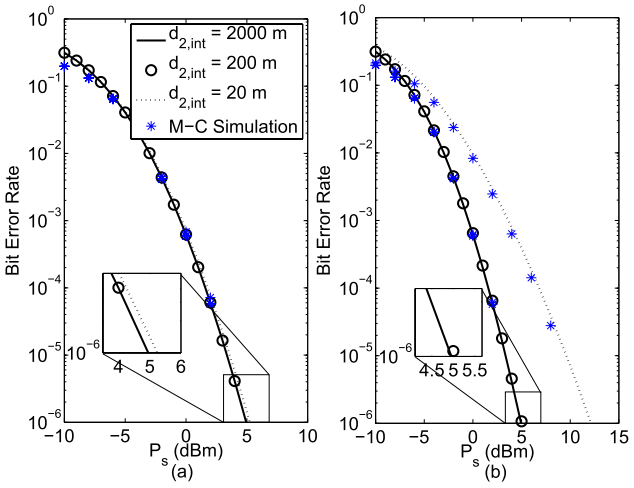

Fig. 8 Upstream transmission: BER versus the average transmitted power per information bit P_s, with $L_{dx,XT} = -30\,\text{dB}$ (a) and $L_{dx,XT} = -15\,\text{dB}$ (b); $C_n^2 = 5 \times 10^{-15}$, $M = 4$, $N = 1$, $L = 4\,\text{km}$.

ulation order M of PPM scheme. Fig. 6(b) shows BER versus L by fixing $N = 3$ and increasing M to investigate the achievable performance improvement of M-PPM. The distances achieved by employing $M = 4$, $M = 8$, $M = 16$, and $M = 32$ are 5 km, 6.1 km, 6.9 km, and 7.5 km, respectively. The distance improvements tend to decrease when higher orders M are employed. This is because the pulses are shortened with high values of M, which are more affected by the pulse broadening due to atmospheric turbulence.

Figure 7 depicts BER versus the transmission bit rate R_b in Gbps with $P_s = 0\,\text{dBm}$ and $L = 4\,\text{km}$ for different PPM modulation orders M in cases of $N = 1$ (Fig. 7(a)) and $N = 2$ (Fig. 7(b)). It is seen that higher transmission rates are achieved by increasing M. More specifically, in Fig. 7(a), at BER $= 10^{-6}$, we can achieve $R_b = 2\,\text{Gbps}$ with 16-PPM and $N = 1$. On the other hand in Fig. 7(b), much higher R_b is reached by adding one more relay (i.e., $N = 2$). For example, $R_b = 6.5\,\text{Gbps}$ can be achieved with 8-PPM at BER $= 10^{-6}$, which means 4.5 Gbps higher than the case of one relay with 16-PPM.

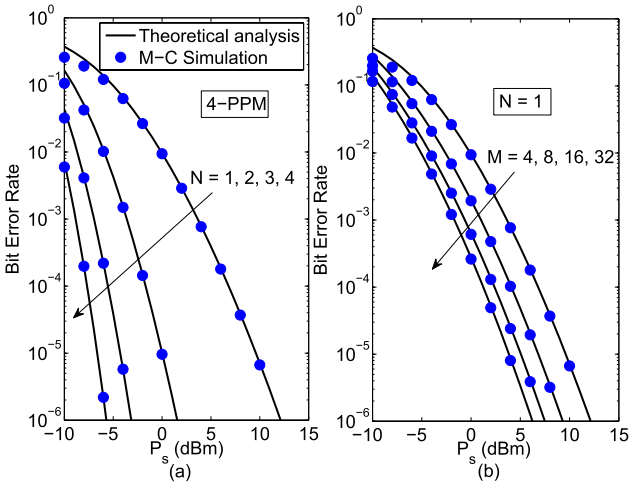

Fig. 9 Upstream transmission: BER versus the average transmitted power per information bit P_s, with different numbers of relays N (a) and different PPM modulation orders M (b); $L_{dx,XT} = -15\,\text{dB}$, $d_{N+1,int} = 20\,\text{m}$, $C_n^2 = 5 \times 10^{-15}$, $L = 4\,\text{km}$.

5.2 Upstream Transmission

For the upstream transmission, in the $(N + 1)$-th hop, the distances from the desired user (signal) and unwanted user (interferer) to the RN are respectively denoted as $d_{N+1,sig}$ and $d_{N+1,int}$. Figure 8 shows the impact of interchannel crosstalk on the upstream transmission by evaluating BER versus P_s within the transmission distance of 4 km with $N = 1$ (i.e., $d_{2,sig} = 2000\,\text{m}$), for different FSO link lengths from the interferer to the RN $d_{2,int}$ in two cases, using good demux ($L_{dx,XT} = -30\,\text{dB}$) and poor demux ($L_{dx,XT} = -15\,\text{dB}$) devices. If a good demux device is used (Fig. 8(a)), at BER $= 10^{-6}$, the effect of crosstalk is negligible as P_s stays the same in both cases of $d_{2,int} = d_{2,sig} = 2000\,\text{m}$ and $d_{2,int} = 200\,\text{m}$. When the interferer is very close to the RN, i.e., $d_{2,int} = 20\,\text{m}$, the impact of crosstalk is still very small as P_s increases only about 0.2 dB compared to the case when $d_{2,int} = 2000\,\text{m}$ and $d_{2,int} = 200\,\text{m}$. In Fig. 8(b), with a poor demux device, the effect of crosstalk is also fragile when $d_{2,int}$ decreases from 2000 m to 200 m as the required P_s increases only about 0.1 dB. However, when the interferer is closer to the RN, e.g., $d_{2,int} = 20\,\text{m}$, P_s increases nearly 7 dB to achieve BER $= 10^{-6}$, compared to the case of $d_{2,int} = 2000\,\text{m}$. This is due to the meagre performance of the demux together with the severe effect of turbulence-accentuated interchannel crosstalk.

Finally, Fig. 9 shows BER versus P_s for different N (Fig. 9(a)) and M (Fig. 9(b)) in the case of using poor demux devices and the interferer is very close to the RN (i.e., $d_{N+1,int} = 20\,\text{m}$). To deal with the severe effect of turbulence-accentuated interchannel crosstalk, one can either increase the number of relays or the modulation order

of PPM scheme. In Fig. 9(a) with 4-PPM, the system performance is considerably improved when more relays are added. Illustratively, the performance improvements when employing 2, 3, and 4 relays are 11 dB, 16 dB, and 18 dB compared to the case when $N = 1$. On the other hand, Fig. 9(b) shows the performance improvement by increasing M when only one relay is employed. It is observed that the performance gains are 3 dB, 2 dB, and 1 dB when M increases from 4 to 8, 8 to 16, and 16 to 32, respectively. The decrease of the performance gains is due to the pulse broadening effect which becomes more severe when M increases. The efficiency of M-PPM comes at the expense of large spectrum occupancy and additional synchronization difficulty with large-alphabet PPM. Thus, by suitably choosing M-PPM and number of relays N in practical deployment scenarios, the system performance could be significantly enhanced.

6. Conclusion

This paper presented a new concept of full-optical access network that employed OAF relaying FSO systems incorporated with WDM. The novel model took advantage of both all-optical relaying FSO transmission and WDM technique, and it could be easily integrated with fiber optics in metro networks to form a low-cost, reliable, flexible, and high-speed optical network. The numerical results showed that atmospheric turbulence and accumulated background and ASE noises had a severe impact on the performance of the proposed system. Nevertheless, thanks to OAF technique combined with M-PPM modulation, the required P_s could be significantly reduced and the transmission distance was increased. The required P_s corresponding to specific values of BER, transmission distance, and turbulence strength were also quantitatively discussed. Finally, the negative effect of turbulence-accentuated interchannel crosstalk in the upstream transmission was thoroughly evaluated.

Acknowledgment

This research is funded by Vietnam National Foundation for Science and Technology Development (NAFOSTED) under grant number 102.02-2015.06.

References

[1] Q. Liu, C. Qiao, G. Mitchell, and S. Stanton, "Optical wireless communication networks for first- and last-mile broadband access [Invited]," J. Opt. Netw., vol.4, no.12, pp.807–828, Dec. 2005.
[2] V.W.S. Chan, "Free-space optical communications," J. Lightw. Technol., vol.24, no.12, pp.4750–4762, Dec. 2006.
[3] E. Ciaramella, Y. Arimoto, G. Contestabile, M. Presi, A. D'Errico, V. Guarino, and M. Matsumoto, "1.28 terabit/s (32x40 Gbit/s) WDM transmission system for free space optical communications," IEEE J. Sel. Areas. Commun., vol.27, no.9, pp.1639–1645, Dec. 2009.
[4] L.G. Kazovsky, W.-T. Shaw, D. Gutierrez, N. Cheng, and S.-W. Wong, "Next-generation optical access networks," J. Lightw. Technol., vol.25, no.11, pp.3428–3442, Nov. 2007.
[5] M. Forzati, A. Bianchi, J. Chen, K. Grobe, B. Lannoo, C.M. Machuca, J.-C. Point, B. Skubic, S. Verbrugge, E. Weis, L. Wosinska, and D. Breuer, "Next-generation optical access seamless evolution: Concluding results of the European FP7 project OASE," J. Opt. Commun. Netw., vol.7, no.2, pp.109–123, Feb. 2015.
[6] S. Hitam, S.N. Suhaimi, A.S.M. Noor, S.B.A. Anas, and R.K.Z. Sahbudin, "Performance analysis on 16-channels wavelength division multiplexing in free space optical transmission under tropical regions environment," J. Comput. Sci., vol.8, no.1, pp.145–148, 2012.
[7] T. Kamalakis, I. Neokosmidis, A. Tsipouras, T. Sphicopoulos, S. Pantazis, and I. Andrikopoulos, "Hybrid free space optical/millimeter wave outdoor links for broadband wireless access networks," Proc. 2007 IEEE 18th International Symposium on Personal, Indoor and Mobile Radio Communications, pp.1–5, 2007.
[8] A.O. Aladeloba, M.S. Woolfson, and A.J. Phillips, "WDM FSO network with turbulence-accentuated interchannel crosstalk," J. Opt. Commun. Netw., vol.5, no.6, pp.641–651, June 2013.
[9] V.V. Mai and A.T. Pham, "Adaptive rate-based MAC protocols design and analysis for integrated FSO/PON networks," Proc. 2015 IEEE International Conference on Communications (ICC), pp.5007–5012, 2015.
[10] Y. Arimoto, "Compact free-space optical terminal for multi-gigabit signal transmissions with a single-mode fiber," Proc. SPIE, Free-Space Laser Communication Technologies XXI, 719908, vol.7199, 2009.
[11] X. Zhu and J.M. Kahn, "Free-space optical communication through atmospheric turbulence channels," IEEE Trans. Commun., vol.50, no.8, pp.1293–1300, Aug. 2002.
[12] M. Safari and M. Uysal, "Relay-assisted free-space optical communication," IEEE Trans. Wireless Commun., vol.7, no.12, pp.5441–5449, Dec. 2008.
[13] C.K. Datsikas, K.P. Peppas, N.C. Sagias, and G.S. Tombras, "Serial free-space optical relaying communications over gamma-gamma atmospheric turbulence channels," J. Opt. Commun. Netw., vol.2, no.8, pp.576–586, Aug. 2010.
[14] T.V. Pham and A.T. Pham, "Performance analysis of amplify-decode-and-forward multihop binary phase-shift keying/free-space optical systems using avalanche photodiode receivers over atmospheric turbulence channels," IET Commun., vol.8, no.9, pp.1518–1526, June 2014.
[15] S. Kazemlou, S. Hranilovic, and S. Kumar, "All-optical multihop free-space optical communication systems," J. Lightw. Technol., vol.29, no.18, pp.2663–2669, Sept. 2011.
[16] E. Bayaki, D.S. Michalopoulos, and R. Schober, "EDFA-based all-optical relaying in free-space optical systems," IEEE Trans. Commun., vol.60, no.12, pp.3797–3807, Dec. 2012.
[17] M.A. Kashani, M.M. Rad, M. Safari, and M. Uysal, "All-optical amplify-and-forward relaying system for atmospheric channels," IEEE Commun. Lett., vol.16, no.10, pp.1684–1687, Oct. 2012.
[18] P.V. Trinh, N.T. Dang, and A.T. Pham, "All-optical AF relaying FSO systems using EDFA combined with OHL over Gamma-Gamma channels," 2015 IEEE International Conference on Communications (ICC), pp.5098–5103, 2015.
[19] N.T. Dang and A.T. Pham, "Performance improvement of FSO/CDMA systems over dispersive turbulence channel using multi-wavelength PPM signaling," Opt. Express, vol.20, no.24, pp.26786–26797, Nov. 2012.
[20] N.T. Dang, H.T.T. Pham, and A.T. Pham, "Average BER analysis of multihop FSO systems over strong turbulence and misalignment fading channels," Proc. 2013 IEEE/CIC International Conference on Communications in China (ICCC), pp.153–157, 2013.
[21] K. Kiasaleh, "Performance of APD-based, PPM free-space optical communication systems in atmospheric turbulence," IEEE Trans. Commun., vol.53, no.9, pp.1455–1461, Sept. 2005.
[22] S.G. Wilson, M. Brandt-Pearce, Q. Cao, and J.H. Leveque, "Free-space optical MIMO transmission with Q-ary PPM," IEEE Trans. Commun., vol.53, no.8, pp.1402–1412, Aug. 2005.

[23] W. Gappmair, S. Hranilovic, and E. Leitgeb, "Performance of PPM on terrestrial FSO links with turbulence and pointing errors," IEEE Commun. Lett., vol.14, no.5, pp.468–470, May 2010.
[24] E.J. Lee and V.W.S. Chan, "Part 1: Optical communication over the clear turbulent atmospheric channel using diversity," IEEE J. Sel. Areas. Commun., vol.22, no.9, pp.1896–1906, Nov. 2004.
[25] M.A. Al-Habash, L.C. Andrews, and R.L. Phillips, "Mathematical model for the irradiance probability density function of a laser beam propagating through turbulent media," Opt. Eng., vol.40, no.8, pp.1554–1562, Aug. 2001.
[26] S.B. Weinstein, Y. Luo, and T. Wang, The ComSoc guide to passive optical networks: Enhancing the last mile access, John Wiley & Sons, 2012.
[27] D. Nesset, "NG-PON2 technology and standards," J. Lightwave Technol., vol.33, no.5, pp.1136–1143, March 2015.
[28] P.T. Dat, A. Bekkali, K. Kazaura, K. Wakamori, and M. Matsumoto, "A universal platform for ubiquitous wireless communications using radio over FSO system," J. Lightw. Technol., vol.28, no.16, pp.2258–2267, Aug. 2010.
[29] R. Ramaswami and K.N. Sivarajan, Optical Networks — A practical Perspective, 2nd ed., Elsevier, 2002.
[30] I.T. Monroy and E. Tangdiongga, Crosstalk in WDM Communication Networks, Springer US, 2002.
[31] G.P. Agrawal, Fiber Optic Communication Systems, Third ed., John Wiley & Sons, 2002.
[32] C.Y. Young, L.C. Andrews, and A. Ishimaru, "Time-of-arrival fluctuations of a space-time Gaussian pulse in weak optical turbulence: An analytic solution," Appl. Opt., vol.37, no.33, pp.7655–7660, Nov. 1998.
[33] J.W. Goodman, Statistical Optics, Wiley-Inter-Science, Hoboken, NJ, 2000.
[34] W. Zhang, S. Hranilovic, and C. Shi, "Soft-switching hybrid FSO/RF links using short-length raptor codes: Design and implementation," IEEE J. Sel. Areas. Commun., vol.27, no.9, pp.1698–1708, Dec. 2009.
[35] I.B. Djordjevic, "Adaptive modulation and coding for free-space optical channels," J. Opt. Commun. Netw., vol.2, no.5, pp.221–229, May 2010.

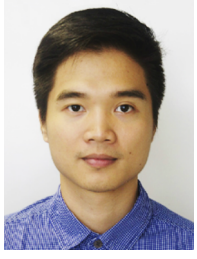

Phuc V. Trinh received the B.E. (First Class Hons.) degree in electronics and telecommunications from the Posts and Telecommunications Institute of Technology, Hanoi, Vietnam in 2013, and the M.Sc. degree in computer science and engineering from the University of Aizu (UoA), Aizuwakamatsu, Japan, in 2015. He is currently working toward the Ph.D. degree in computer science and engineering at UoA. His study in Japan is funded by a Japanese government scholarship (MonbuKagaku-sho). He was the recipient of several awards, including the IEEE Sendai Section's Student Award (2014), the UoA President's Award for the best Master's student (2015), the Young Researcher's Encouragement Award from IEEE VTS Japan Chapter (2015), and the IEEE ComSoc Sendai Chapter Student Excellent Researcher Award (2015). His current research interests are in the area of optical wireless communications, including modulation techniques, coding, system modeling and simulation, and performance analysis. He is a student member of IEICE and IEEE.

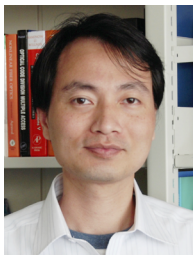

Ngoc T. Dang received the B.E. degree from Hanoi University of Technology in 1999 and the M.E. degree from Posts and Telecommunications Institute of Technology (PTIT), Vietnam in 2005, both in Electronics and Telecommunications. He got the Ph.D. degree in Computer Science and Engineering from the University of Aizu, Japan, in 2010. He is currently Associate Professor/Deputy Head of Department of Optical Communications at PTIT. His present research interests are in the area of communication theory with a particular emphasis on modeling, design and performance evaluation of optical CDMA and optical wireless communication systems.

Truong C. Thang received the B.E. degree from Hanoi University of Technology, Vietnam, in 1997 and Ph.D. degree from KAIST, Korea, in 2006. From 1997 to 2000, he worked as an engineer in Vietnam Post & Telecom (VNPT). From 2007 to 2011, he was a Member of Research Staff at Electronics and Telecommunications Research Institute (ETRI), Korea. He has been an active member of Korean and Japanese delegations to standard meetings of ISO/IEC and ITU-T from 2002. Since 2011, he has been an Associate Professor of the University of Aizu, Japan. His research interests include multimedia networking, image/video processing, content adaptation, IPTV, and MPEG/ITU standards.

Anh T. Pham received the B.E. and M.E. degrees, both in Electronics Engineering from the Hanoi University of Technology, Vietnam in 1997 and 2000, respectively, and the Ph.D. degree in Information and Mathematical Sciences from Saitama University, Japan in 2005. From 1998 to 2002, he was with the NTT Corp. in Vietnam. Since April 2005, he has been on the faculty at the University of Aizu, where he is currently Professor and Head of Computer Communications Laboratory with the Division of Computer Engineering. Professor Pham's research interests are in the broad areas of communication theory and networking with a particular emphasis on modeling, design and performance evaluation of wired/wireless communication systems and networks. He has authored/co-authored more than 140 peer-reviewed papers, including 40+ journal articles, on these topics. Professor Pham is senior member of IEEE. He is also member of IEICE and OSA.